Exp Fluids (2013) 54:1439
DOI 10.1007/s00348-012-1439-5

RESEARCH ARTICLE

Hummingbirds generate bilateral vortex loops during hovering: evidence from flow visualization

Sam Pournazeri · Paolo S. Segre · Marko Princevac · Douglas L. Altshuler

Received: 1 March 2012 / Revised: 4 November 2012 / Accepted: 10 December 2012 / Published online: 25 December 2012

Abstract Visualization of the vortex wake of a flying animal provides understanding of how wingbeat kinematics are translated into the aerodynamic forces for powering and controlling flight. Two general vortex flow patterns have been proposed for the wake of hovering hummingbirds: (1) The two wings form a single, merged vortex ring during each wing stroke; and (2) the two wings form bilateral vortex loops during each wing stroke. The second pattern was proposed after a study with particle image velocimetry that demonstrated bilateral source flows in a horizontal measurement plane underneath hovering Anna's hummingbirds (*Calypte anna*). Proof of this hypothesis requires a clear perspective of bilateral pairs of vortices. Here, we used high-speed image sequences (500 frames per second) of *C. anna* hover feeding within a white plume to visualize the vortex wake from multiple perspectives. The films revealed two key structural features: (1) Two distinct jets of downwards airflow are present under each wing; and (2) vortex loops around each jet are shed during each upstroke and downstroke. To aid in the interpretation of the flow visualization data, we analyzed high-speed kinematic data (1,000 frames per second) of wing tips and wing roots as *C. anna* hovered in normal air. These data were used to refine several simplified models of vortex topology. The observed flow patterns can be explained by either a single loop model with an hourglass shape or a bilateral model, with the latter being more likely. When hovering in normal air, hummingbirds used an average stroke amplitude of 153.6° (range 148.9°–164.4°) and a wingbeat frequency of 38.5 Hz (range 38.1–39.1 Hz). When hovering in the white plume, hummingbirds used shallower stroke amplitudes ($\bar{x} = 129.8°$, range 116.3°–154.1°) and faster wingbeat frequencies ($\bar{x} = 41.1$ Hz, range 38.5–44.7 Hz), although the bilateral jets and associated vortices were observed across the full kinematic range. The plume did not significantly alter the air density or constrain the sustained muscle contractile frequency. Instead, higher wingbeat frequencies likely incurred a higher metabolic cost with the possible benefit of allowing the birds to more rapidly escape from the visually disruptive plume.

Sam Pournazeri and Paolo S. Segre contributed equally to the work.

Electronic supplementary material The online version of this article (doi:10.1007/s00348-012-1439-5) contains supplementary material, which is available to authorized users.

S. Pournazeri · M. Princevac
Department of Mechanical Engineering, University of California Riverside, Riverside, CA 92521, USA

P. S. Segre · D. L. Altshuler
Department of Biology, University of California Riverside, Riverside, CA 92521, USA

P. S. Segre · D. L. Altshuler (✉)
Department of Zoology, University of British Columbia, Vancouver, BC V6T 1Z4, Canada
e-mail: doug@zoology.ubc.ca

1 Introduction

Research in animal aerodynamics has demonstrated that the wake patterns, which can be visualized with increasing detail, differ among species and by flight mode. Comparisons across forward flight speeds in bats, birds, and insects have revealed both differences and some examples of convergence. The general pattern described for birds has been that the wake produced by the wings is connected over the body, generating a single vortex loop at slow speeds and changing circulation at higher speeds (Kokshaysky 1979; Spedding et al. 1984, 2003; Spedding 1987).

Bats, in contrast, have been shown to generate bilateral vortex wakes—one per wing—at slow speeds and more continuous shedding at moderate speeds (Hedenström et al. 2007; Muijres et al. 2008). Both patterns have been seen in insects, with hawkmoths producing one vortex wake (Bomphrey et al. 2005) and bumblebees producing bilateral wakes (Bomphrey et al. 2009). Particle image velocimetry (PIV) methods have improved in temporal and spatial resolution over the last few years as have the coverage of species of different sizes and flight modes. One of the significant additions to the emerging model of the wakes of flying animals is that vortices can be shed from the wing roots in both birds and bats over a wide range of sizes and flight speeds, although the strength and persistence of these root vortices varies by species and speed (Hedenström et al. 2009; Johansson and Hedenström 2009; Hubel et al. 2010, 2012; Henningsson et al. 2011; Muijres et al. 2011, 2012). The presence of root vortices indicates that if and when the body is included in producing vertical force, this requires some time to develop. Other aerodynamic consequences of root vortices are still to be demonstrated, but the Kutta–Joukowski and Kelvin–Helmholtz theorems indicate that these shedding patterns will lead to differences in lift-generating mechanisms and the energetic cost of flight (Rayner and Gordon 1998; Hedenström et al. 2007).

Hovering flight is useful for examining the relationships between animal performance and its aerodynamic wake because in the absence of forward flight the sources of the wake are restricted to the wings and the wake interactions with the body. Several features of the flow around hummingbird wings have been well described (Warrick et al. 2005, 2009), but a thorough description of the wake topology is not available. It had been proposed that a hovering hummingbird generates one vortex ring per stroke (Rayner 1979; Ellington 1984; Pennycuick 1988; Rayner and Gordon 1998), which would match the vortex shedding pattern proposed for larger birds during slow flight (Spedding et al. 1984, 2003). Altshuler et al. (2009) made PIV measurements in a horizontal plane beneath the hummingbirds close to the tail. These measurements revealed source flows induced by vortices, which appeared on each side of the animal at an interval of double the wingbeat frequency. They proposed that each wing of a hovering hummingbird generates its own vortex loop during each downstroke and upstroke. However, they did not have images of the vortices. One prediction of the proposed wake topology is that there should be bilateral jets, one per wing.

Hovering presents at least two challenges for PIV recordings. In the absence of forward speed, the wake does not trail behind but instead piles up beneath the animal, which can cause the vortices to occur very close to and possibly be occluded by the body at low wake stream velocities. Also, because the wings are active during both up- and down-stroke, each stroke can disrupt previous stroke's wake. One solution to these problems is to compile a time-resolved history of the flow field (Bomphrey et al. 2006). However, for hovering animals, sequential measurement of the vortex progression over the course of a single stroke requires a specialized fast response PIV system.

Previous PIV studies with hovering hummingbirds used 2D approaches that included descriptions of flows around cross-sections of the wing and thin slices from the lateral, rear, and underneath perspectives (Warrick et al. 2005, 2009; Altshuler et al. 2009). Proof of the bilateral vortex loop model requires a perspective of the 3D flow, which can be obtained by visualization of the flow field. Here, we present the results from films of hovering hummingbird in a white plume emitted by the heating of dry ice. Additional high-speed videography from multiple perspectives was used to describe the position, velocity, and phase relationships of the wing tips and wing roots in normal air. These kinematic data were used to refine four different vortex topologies for comparison with the visualized structures. The topologies differ with respect to the number of jets (i.e., one vs. two) per stroke and the connections of the wakes (i.e., via the wingtip or wing root).

2 Methods

2.1 Animals

Six male Anna's hummingbirds (*Calypte anna*) were captured on the campus of the University of California, Riverside (UCR), and used for the flow visualization measurements. Another four male *C. anna* were captured on the campus of the California Institute of Technology (Caltech) for the wingbeat kinematic measurements. The hummingbirds were housed in campus vivarium, trained to feed from artificial feeders, and fed a diet of sugar water and specially formulated hummingbird nectar (NEKTAR-Plus, NEKTON GmbH). At the conclusion of the experiments, all of the birds were banded and released at the original site of capture. All procedures were approved by the UCR and Caltech Institutional Animal Care and Use Committees.

2.2 Flow visualization

The flow visualization measurements were made between January and March 2011 at UCR. The flight chamber (0.5 m × 0.6 m × 0.6 m) was constructed with two clear acrylic sides for filming, two black cardboard sides to increase contrast with the background, and a mesh floor

and ceiling to allow air circulation. We trained the hummingbirds to hover at a feeder in the center of the chamber surrounded by a white plume, which allowed for visualization of the wake patterns. The plumes were formed by adding dry ice to hot water above the cage. The water temperature accelerated the sublimation process and resulted in a plume that entered the cage through the mesh top, enveloped the bird, and exited through the bottom of the cage. The plume extended only ~5–15 cm around the feeder so that the bird could enter and exit it at will. We filmed the region in front of the feeder from the side and rear perspectives using two synchronized high-speed digital cameras (Fastec Imaging Troubleshooter, Vision Research Miro 4) recording at 500 frames per second. Both cameras used the tip of the feeder as the main point of focus. We recorded eight trials for each bird, and each trial's videos contained ~150 wingbeat cycles. The visibility of the vortices associated with the wake structures depended upon their position and orientation relative to the camera. However, each of the six birds approached the feeder from a slightly different angle, so every video essentially provided a unique view of the wake structures.

2.3 Wingbeat kinematics

The wingbeat kinematic measurements were made between December 2003 and April 2006 at Caltech. The acrylic flight chamber (1 m × 1 m × 1 m) had three white sides and three clear sides for filming with three high-speed cameras (Photron APX). We trained the hummingbirds to hover feed from a small artificial feeder located in the center of the chamber. The three cameras recorded at 1,000 frames per second. Points at the wingtips, shoulder, and the wing root were digitized frame by frame using DLTdv software (Hedrick 2008) running in the Matlab platform (MathWorks Inc., Natick, MA). A multi-point calibration object was filmed immediately before and after flight trials. We analyzed one hovering sequence for each bird.

The wing stroke angles were calculated from Cartesian coordinates of the digitized anatomical landmarks in 3D space. The position angle ϕ is defined as the angle between the projection of the wingtip or wing root into the horizontal plane and a line defined by the midpoint between the wingtips at pronation and the head. The values span from 0°, directly behind the bird, to 180°, directly in front of the bird. The elevation angle θ is defined as the angle between the wingtip or wing root, the shoulder, and the projection of the wingtip or wing root into the horizontal plane. The values span from −90°, directly below the bird, to +90°, directly above the bird, with 0° at the horizontal position. The downstroke period T_D is defined as the time from the rearward most excursion of the position angle to the forward most excursion of the position angle in a given wingbeat. The upstroke period T_U is the time from the forward to the rearward most excursion within each wingbeat. The downstroke ratio τ is defined as T_D/T, where T is the wingbeat period.

The 3D positions of the body and wing points were imported to a 3D modeling program (sketchup.google.com) to generate four simplified versions of the single and bilateral vortex topologies. The most likely topology was oriented to match with the body orientation and wing positions of the hummingbird in the plume to assist in the identification of flow structures.

2.4 Vortex terminology

We present terminology to describe the observations from the flow visualization experiment. It is now recognized that vortex wakes are complex, interconnected structures (Spedding et al. 2003), so labeling specific segments as discrete vortices is an oversimplification that is useful for comparison in the absence of a completely resolved flow field. When possible, we have used existing terminology, but we have also had to modify some terms to match the observed structures. Three distinct families of vortices are defined: (1) structures shed from the wing tip, (2) from the wing root, and (3) during stroke reversal.

Wingtip vortices are formed by the pressure differences above and below the wing. This pressure difference induces a flow around the wing (Green 1995), which forms into a vortex that is shed off the wingtip during the progression of the stroke. Following the Prandtl lifting-line theory (Anderson 1991), these vortices can also be explained through the shed of the rolled-up streamwise vorticity that is generated due to the spanwise variation of bound circulation (i.e., lift), which is a result of the finite spanwise length of the wing (three-dimensional effects).

Wing root vortices are observed near the wing root. Wing root vortices are generated through a similar mechanism as wingtip vortices, where streamwise vorticity of opposite spin rolls up into a distinct vortex. These vortices have been observed in insects, birds, and bats with varying strength and persistence (Hedenström et al. 2007, 2009; Muijres et al. 2008; Muijres et al. 2011, 2012; Bomphrey et al. 2009; Johansson and Hedenström 2009; Hubel et al. 2010, 2012; Henningsson et al. 2011). The cause and function of these vortices has not been fully established.

At the termination of each stroke, the wing sheds a vortex that can be caused by several sources. Due to a rapid change in translational velocity (deceleration), and assuming that the change in the descending velocity along the wing chord is negligible, a region with a significantly high velocity gradient (i.e., high vorticity) is developed at the leading edge of the wing. As the vorticity rolls up in the wake, it forms a stopping vortex with the same sign as the

bound vortex that is shed as the wing tip reverses (Anderson 1991; Warrick et al. 2005, 2009; Hedenström et al. 2007). Additional sources can include changes in the angle of attack and camber, which lead to variation in bound circulation, thereby causing vortex shedding. During the initiation of the next stroke when the wing undergoes an acceleration in the opposite direction, a starting vortex is formed, which is rotating in the opposite direction to the new bound vortex of the wing but in the same direction as the stopping vortex from the previous stroke. Because we did not observe separate stopping and starting vortices, we use the term *reversal* vortex to refer to what may be the combination of the two structures. *Reversal* vortices occur at the beginning and ending of each stroke, so we use the terms *pronating* and *supinating reversal* vortices to distinguish the vortices that occur behind and in front of the bird, respectively.

3 Results

3.1 Flow visualization

The videos of hummingbirds hovering within the white plume demonstrate clear development of flow structures. We first describe a sequence of plume entrainment on the left side of a hummingbird (Bird 6, trial 5, online supplementary video S1). Seven successive frames (59–65) from this video depict the first half of a downstroke (Fig. 1). The panels on the left are raw images, whereas the panels on the right are the exact same images but with arrows illustrating the location and direction of prominent flow structures.

After the wing pronates at the end of the upstroke and start of the downstroke (frame 60), a counterclockwise pronating reversal vortex is shed. As the wing continues its stroke, a wingtip vortex is shed, first visible in frame 63. This vortex is formed as a result of the roll-up of the streamwise vorticity that is shed from the wing. The wingtip vortex occurs throughout the entire course of the downstroke. However, in the video, it only becomes clearly visible as a vortex when its cross-section is perpendicular to the camera (frame 63), and it continues to show up until the vortex vector becomes almost in line with the image plane. The pronating reversal and wingtip vortices form a continuous horizontal loop that induces a strong vertical jet-shaped like an hourglass, converging above and diverging below the wing.

We next take advantage of multiple perspectives of the birds' positions with respect to the plume to describe additional flow features (Fig. 2). The beginning of the third trial of bird 6 provides a clear perspective of a train of vortex loops on the right side of the animal (online

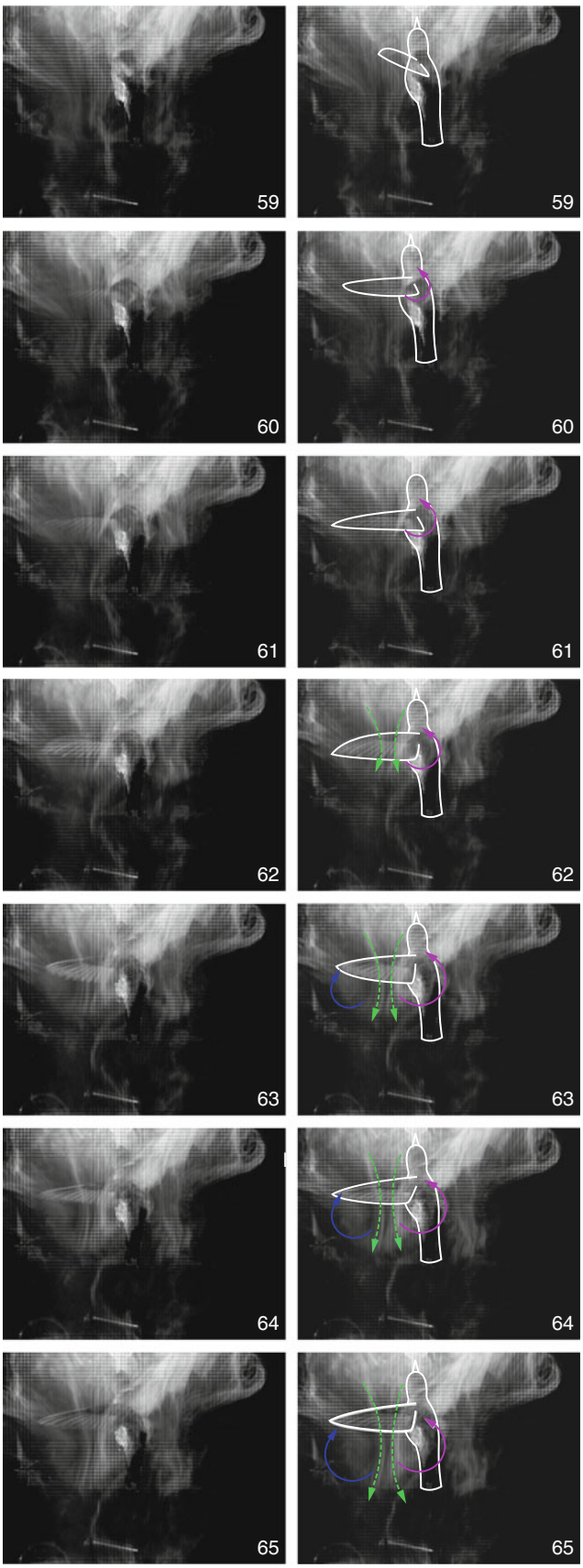

◀ **Fig. 1** Flow visualization of a hovering hummingbird from the rear-left perspective, demonstrating sequential development of a vortex loop on the left side during a downstroke. The time interval between frames is 2 ms and sequence runs from top to bottom. The panels on the *left* are unmanipulated images. The panels on the *right* are the same images but with the bird outlined in *white* and key features of the flows indicated by color: *blue* (downstroke wing tip vortex), *purple* (reversal vortex), *green* (air jet). This image sequence comes from frames 59–65 (labeled in the *lower right* of each panel) of the online video (S1) of trial #5 from bird 6

supplementary video S2). Several structures are visible in frame 101 (Fig. 2a, b). This frontal perspective of the bird is shown immediately after wing pronation. The wingtip vortex created by the previous upstroke is visible (b1), as well as both the supinating reversal (b2) and wingtip (b3) vortices created by the previous downstroke. The large wingtip vortex created by two downstrokes earlier is also visible (b6), but the smaller supinating reversal (b5) and wingtip (b4) vortices from the previous upstroke have already dissipated. The straight arrows represent the extrapolated location of the dissipated vortices.

Later in the same video, the plume has expanded and the bilateral jets and associated vortex loops shed from the wings are visible (Fig. 2d, e). This image is also a frontal view of the bird immediately after wing pronation. The wingtip vortices from the previous downstroke (e1 and e2) and the right supinating reversal vortex (e3) are visible. The supinating reversal vortex for the left wing is not visible, although its hypothesized location is indicated (e4). The left and right wings have generated individual jet streams (e5 and e6).

A wider field of view of the rear perspective of a hummingbird hovering in the plume is available for the second trial of bird 5 (online supplementary video S3). Frame 58 (Fig. 2g, h) occurred at the start of the downstroke and contains a view of both the pronating reversal (h1) and wingtip (h2) vortices created by the previous downstroke. It also provides a clear view of the shape of the vortex tube (h3) connecting the vortices.

The lateral perspective of the wake structure from a hovering hummingbird has been described in previous PIV studies (Warrick et al. 2005, 2009), and we provide that perspective here (online supplementary video S4) for comparison. At frame 37, the reversal vortices are parallel or nearly so with respect to the camera plane and, therefore, not visible. The wingtip vortices from both the upstroke and the downstroke are visible. Two sets of vortices can be observed at stroke transition: k1 is the wingtip vortex shed at the beginning of the current upstroke, and k2 is the wingtip vortex shed at the end of the previous downstroke (Fig. 2j, k). At the previous upstroke–downstroke transition, there is a single vortex (k3), which is likely to contain the wingtip vortices that have either merged by this point or are too close to be resolved. At the previous downstroke–upstroke transition, the wingtip vortex from the downstroke is still prominent (k5), but the wingtip vortex from the upstroke has just disappeared. The red arrow indicates its hypothesized position (k4). The previous upstroke–downstroke vortex (k6) has now dissipated.

3.2 Kinematics experiment

The wing stroke amplitude (Φ), wingbeat frequency (f), and downstroke ratio (τ) of the hummingbirds from both experiments are presented in Table 1. The hummingbirds in the kinematics experiment exhibited values for these variables that are similar to what has previously been reported for male *C. anna* during hovering (Altshuler et al. 2010b). On average, the hummingbirds in the flow visualization experiment used lower stroke amplitudes and higher wingbeat frequencies, but the individual birds were also more variable. Bird 4, for example, used a stroke amplitude/wingbeat frequency combination that was nearly identical to the average values for the kinematics experiment. An image sequence of flow development on the left side of the bird is presented in Fig. 3 and in online supplementary video S5. The vortex dipole in frame 351 consists of a wingtip vortex on the left and either a reversal or wing root vortex on the right. From this perspective of the bird, both are possible because the position at which pronation occurred was nearly perpendicular to the image plane of the camera.

The average instantaneous position (ϕ) and elevation (θ) angles of the left and right wing tips and wing roots are depicted in Fig. 4. The position angles of the wingtips and wing roots have similar amplitudes, but with the wingtips leading at all stages of the stroke. The elevation traces exhibit a double harmonic pattern, but again with the wing tips leading at all phases. Thus, the wing root reverses in both position and elevation after the wing tip. The left and right wings followed nearly identical patterns.

3.3 Wake pattern

The wingbeat kinematics and flow visualizations were used to visualize four potential topologies for hovering hummingbirds. These new but still simplified models are based upon previous hypotheses of the single (Rayner 1979) and bilateral (Altshuler et al. 2009) vortex loops and other possible explanations for the flow patterns observed here (Fig. 5). The wing stroke is assumed to impart the same downward momentum to the vortices in all four models. The downward velocity was estimated by tracing wingtip vortices over sequences of images in the flow visualization experiment. The images were calibrated using a ruler that was placed vertically next to the feeder and filmed

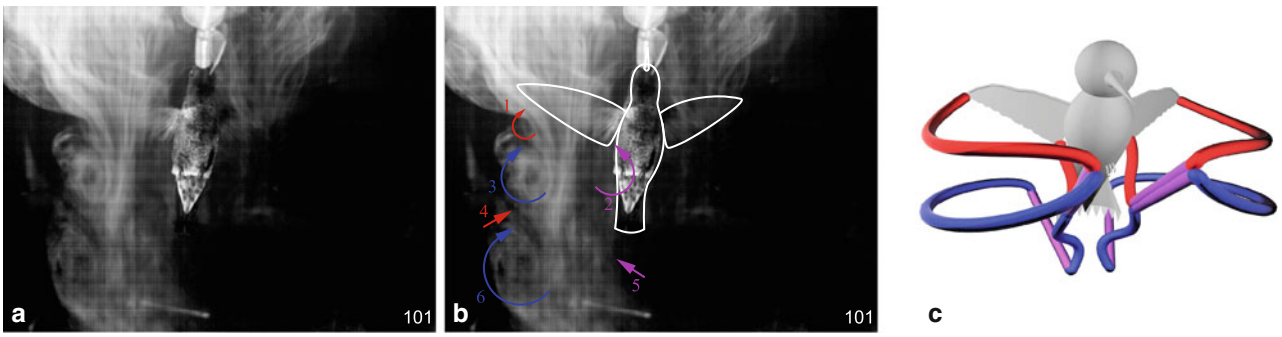

Video S2: bird 6, trial 3

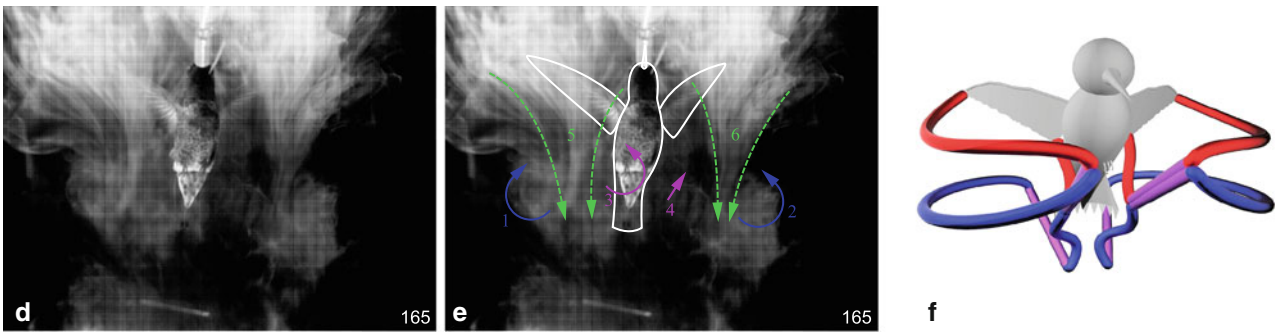

Video S2: bird 6, trial 3

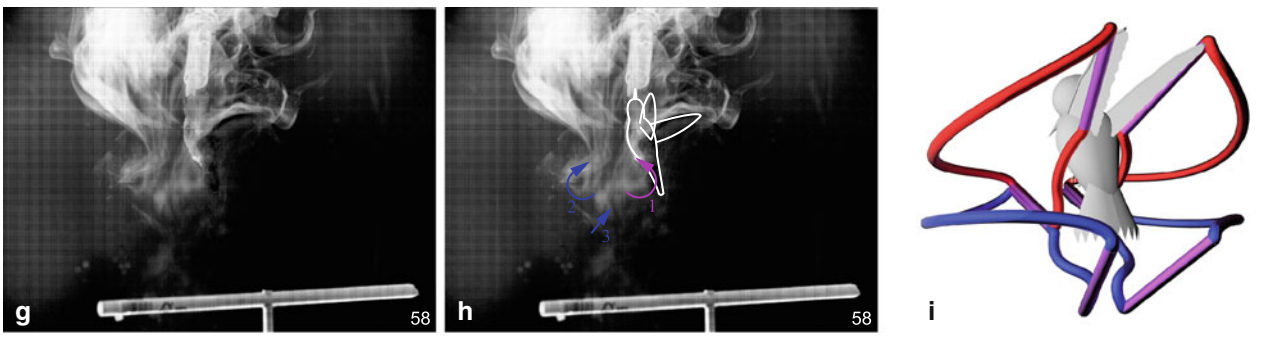

Video S3: bird 5, trial 2

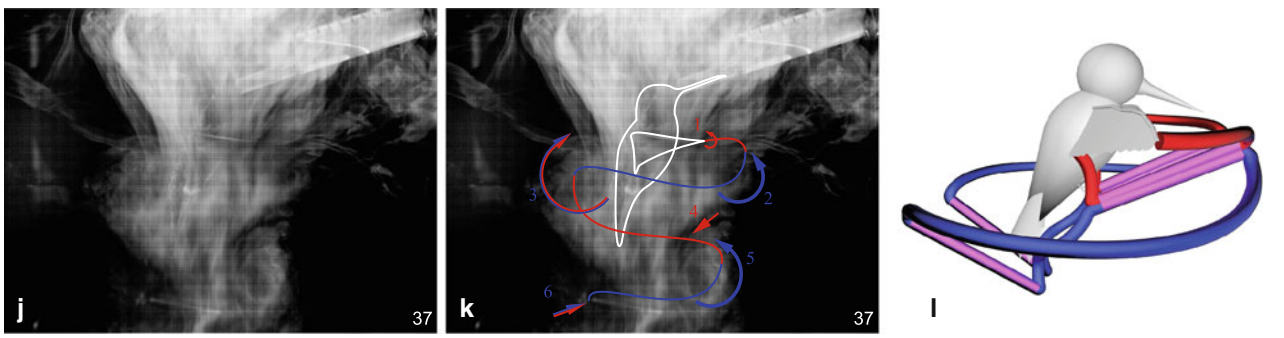

Video S4: bird 6, trial 9

Fig. 2 Visualization of the vortex wake from multiple perspectives. Unmanipulated images are presented in the *left* panels. The *central* panels contain the same images with the bird outlined in *white* and key features of the flows indicated by color: *blue* (downstroke wingtip vortex), *red* (upstroke wingtip vortex), *purple* (reversal vortex), *green* (air jet). *Straight arrows* indicate the hypothesized locations or structures that are no longer present. The numbers build from most recent (1) to oldest (highest number) shedding events. The accompanying online video names, bird numbers, and trial are provided underneath the *left* panels. The bilateral vortex model has been placed in similar orientations for comparison in the *right* panels. The frontal perspective is presented after a supinating rotation (**a**, **b**) and then again at the beginning of downstroke (**d**, **e**). An off-axis rear perspective with a wide field of view is presented for a wing at the initiation of a downstroke (**g**–i). A lateral view is presented at mid-downstroke with the wingtip paths during the down- and up-strokes indicated in *blue* and *red*, respectively (**g**–**l**)

Table 1 Wingbeat kinematics of hummingbirds used in the flow visualization and kinematic experiments

Bird #	n_Φ	Φ (°)	$n_{f,\ \tau}$	f (Hz)	τ (%)
Flow visualization					
3	10	116.32 (1.03)	33	41.56 (0.37)	44.98 (0.63)
4	10	154.08 (0.98)	26	38.51 (0.29)	46.45 (0.37)
5	10	121.55 (0.86)	21	44.73 (0.33)	45.92 (0.41)
6	10	127.05 (1.09)	21	39.55 (0.39)	50.37 (0.64)
$\bar{x}$		129.75 (8.40)		41.09 (1.37)	46.93 (1.18)
Bird #	n	Φ (°)		f (Hz)	τ (%)
Kinematics					
7	15	148.94 (1.17)		39.08 (0.20)	50.00 (0.34)
8	11	164.38 (0.91)		38.62 (0.31)	46.29 (0.43)
9	14	149.36 (0.96)		38.05 (0.18)	49.72 (0.48)
10	14	151.65 (0.54)		38.27 (0.26)	47.26 (0.33)
$\bar{x}$		153.58 (3.65)		38.51 (0.22)	48.32 (0.91)

The sample sizes (n) refer to the number of wingbeats analyzed to determine the wing stroke amplitude (Φ, in degrees), wingbeat frequency (f, in hertz), and downstroke ratio (τ, in %). For the flow visualization measurements, the sample size of wingbeats analyzed was lower for the stroke amplitude than for the other variables. The experiment average by type of measurement is indicated by $\bar{x}$ with standard errors in parentheses. Rows with bird numbers contain individual means with standard errors in parentheses

immediately after the experiment. The calibration was then applied to the flow visualization images and analyzed using ImageJ. The average descent velocity based on 60 wingbeats from six individuals was 2.6 m/s (±0.2 m/s SD). This velocity is a coarse approximation and was not used to calculate aerodynamic force and efficiency.

The outer paths of the models follow the paths of the wing tips over the stroke amplitudes recorded during hovering flight in the kinematics measurements. For the merged vortex ring model (Fig. 5a), the wingtip vortex path follows an extrapolated wingtip trajectory to merge the left and right sides. The indented merged vortex loop model is a version of the single loop model that includes reversal vortices. It assumes that the connection between the left and right sides occurs near the body, which produces an hourglass-shaped loop (Fig. 5b). The bilateral vortex loops model accounts for the reversal vortices by assuming that these are connected by root vortices (Fig. 5c). Because we did not observe separate starting and stopping vortices, these are assumed to either merge or appear very close together in this and the indented merged vortex loop model. The bilateral vortex loops model was oriented to match each of the bird positions in Fig. 2, where it is presented in the right column. The concentric vortex rings model is presented for the scenario in which the stroke amplitude is close to 180°, and the wingtips and wing roots each form closed loops unifying the left and right sides (Fig. 5d). Three-dimensional animations of the four topologies are available in the online supplementary materials (videos S6–S9).

4 Discussion

4.1 Flow visualization

Previous PIV measurement of the horizontal plane underneath hovering Anna's hummingbirds, *C. anna*, provided vector topologies that implicated the presence of bilateral vortex loops in the wake (Altshuler et al. 2009). However, only the source flows caused by the jets could be distinguished and not the associated vortices. Here, we made high-speed image sequences of the wake structures formed by *C. anna* hovering in white plumes. Videos recorded from rear (Figs. 1, 2g) and frontal (Fig. 2a, d) perspectives revealed the presence of bilateral jets and associated vortices, which disproves the merged vortex ring model (Fig. 5a), at least for this species of hummingbird. There are two potential topologies that can account for observations by the previous PIV study (Altshuler et al. 2009) and the current flow visualization: an indented merged vortex loop (Fig. 5b) and the bilateral vortex loop models (Fig. 5c).

The difference between the models that include bilateral jets is the presence or absence of root vortices. Vortex dipoles surrounding the bilateral jets were shed during both up- and down-strokes. However, because of the proximity and alignment of the root and reversal vortices at the start and end of the stroke, it is not certain which structure was visualized in each frame. Assuming that there are no root vortices, the most common wake structure expected would be the topology suggested by Spedding et al. (2003) where the body is included in the lift generation. This can be valid in forward flight. However, the distinct feature of hovering flight compared to other flight modes is the absence of forward flight speed, which essentially excludes the body from the lift generation. The flow speed across the wing will increase with distance from the body but should be zero at the wing-body junction. This decrease in flow speed, which is also a decrease in circulation toward the body, should be accompanied by a vortex shed close to the root. The total excursion of the wing root during normal hovering is considerably less than the length of the body, making it highly implausible that the vortices shed from the left and right wing roots connect to each other. Rather, this root vortex should connect the supinating and pronating vortices from the same wing. This will form a closed loop and lead to a bilateral vortex wake structure.

The two potential topologies with bilateral jets (5b,c) include the assumption that the vortices produced by each

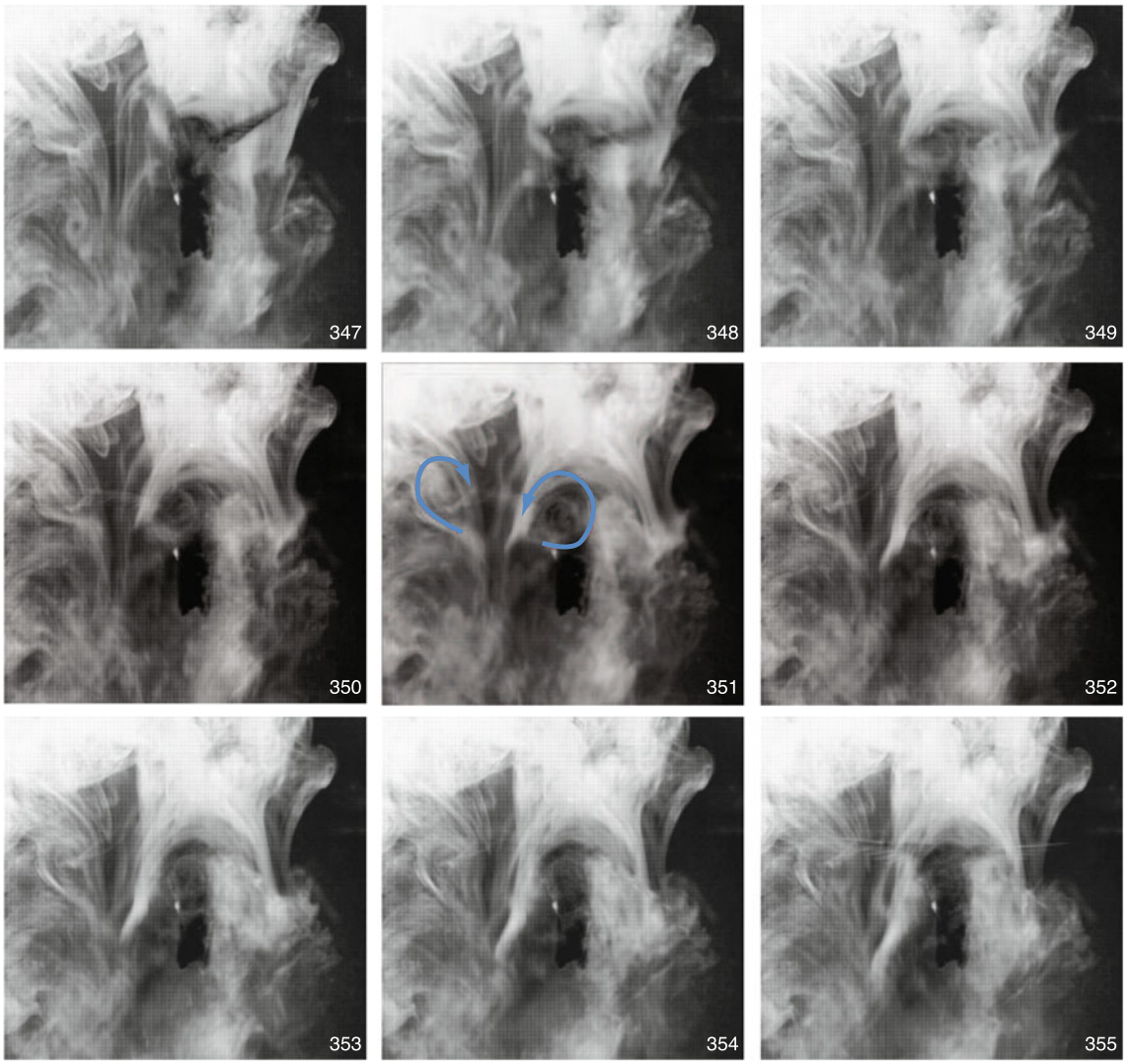

Fig. 3 Image sequence of a hummingbird hovering in the plume with wingbeat frequency and wing stroke amplitude values that fall within the range of birds hovering in normal air. The development and progress of a jet including shed wing tip and either reversal or wing root vortices during the downstroke is visible on the *left* side of the animal. The vortices are indicated by *blue arrows* in frame 351. The amplitude of this specific downstroke was 146°

stroke form connected streams rather than separate structures. We did not discern separate stopping and starting vortices, which is consistent with the flow patterns generated at the downstroke–upstroke transition (supination), but not of the upstroke–downstroke transition (pronation) reported for Rufous hummingbirds, *Selasphorus rufus* (Warrick et al. 2009) (see Warrick et al. 2009 supplementary material, Fig. 6). Because the transition at both supination and pronation occurs very fast relative to the descent rate of the flow passing the bird, these vortices are spatially very close and, it appears, merge to form a single vortex. The wake created by a hovering *C. anna* should, therefore, consist of a vertically connected vortex ladder rather than separated vortex loops. It is unknown whether the wing–wake interactions at stroke transition include strong components of wing rotation and wake capture (Dickinson et al. 1999).

The vortex structure influences the lift generated by the wings. The wake patterns of Blackcaps *Sylvia atricapilla* (Johansson and Hedenström 2009) include wing root vortices that could be either opposite or same sign relative to the wingtip vortices. The upwash and downwash induced by these vortices can reduce or enhance the lift, respectively (Wang and Wu 2010). In the present study, we observed vortex dipoles under each wing with the outer (wingtip) pole always of opposite sign to the inner (reversal or wing root) pole. This suggests that a wing root vortex generates upwash directly beneath the hummingbird. This structure can be seen in image sequences presented here (e.g., Fig. 2d, e), and its signature also exists in PIV results

presented in Altshuler et al. (2009) as a sink flow behind the bird body (e.g., their Fig. 8). Although the upwash between the bilateral loops is relatively weak, it can slightly reduce the total lift by generating a local negative lift. Thus, when all else is equal, the single vortex loop will produce higher aerodynamic force due to the larger downwash area, absence of the upwash, and inclusion of the body in lift generation. For a hovering animal, the vertical force must by definition balance the body weight regardless of wake topology, but the single vortex ring wake will be more aerodynamically efficient (Norberg et al. 1993; Muijres et al. 2012).

Animals attempting to maximize lift should expand the area of downwash, whereas animals aiming to minimize power expenditure would benefit from producing the wake that meets the aerodynamic requirements for the smallest muscle output. A potential advantage of each wing producing a vortex loop is that differences in the size and orientation of the wake could confer enhanced ability to produce left–right asymmetries in aerodynamic force (Bomphrey et al. 2009). This level of control would be advantageous for maneuverability (Henningsson et al. 2011), potentially at the expense of stability.

The original vortex model for hovering in hummingbirds (Fig. 5a) was based on early measurements from a tropical hummingbird (*Florisuga fuscus*) that used a relatively high stroke amplitude and close to horizontal stroke plane (Stolpe and Zimmer 1939). Although necessarily simplistic, this model of a merged vortex ring (Rayner 1979; Ellington 1984; Pennycuick 1988; Rayner and Gordon 1998), such as that produced by helicopters, allowed for consideration of how aerodynamics could influence the metabolic costs of hovering flight (Epting and Casey 1973) and related ecological and biogeographical constraints (Feinsinger and Chaplin 1975; Feinsinger and Colwell

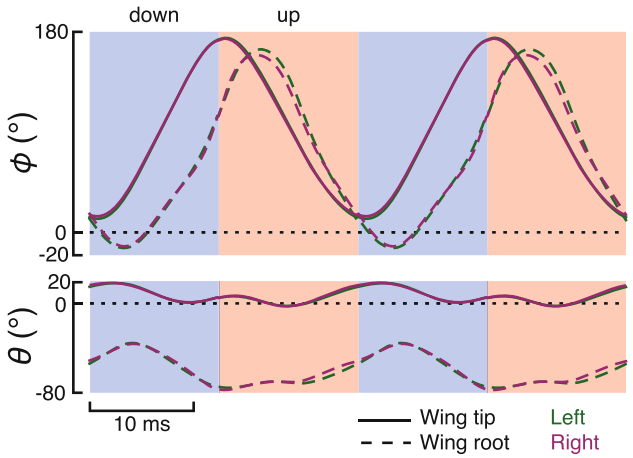

Fig. 4 The average instantaneous wing position (ϕ) and elevation (θ) angles of the wing tips and wing roots from free flight measurements of four male Anna's hummingbirds (*Calypte anna*) during hovering flight. The downstroke phase is indicated in *light blue* and the upstroke is in *light red*. The mean stroke kinematic pattern is presented twice in succession for viewing the stroke transitions

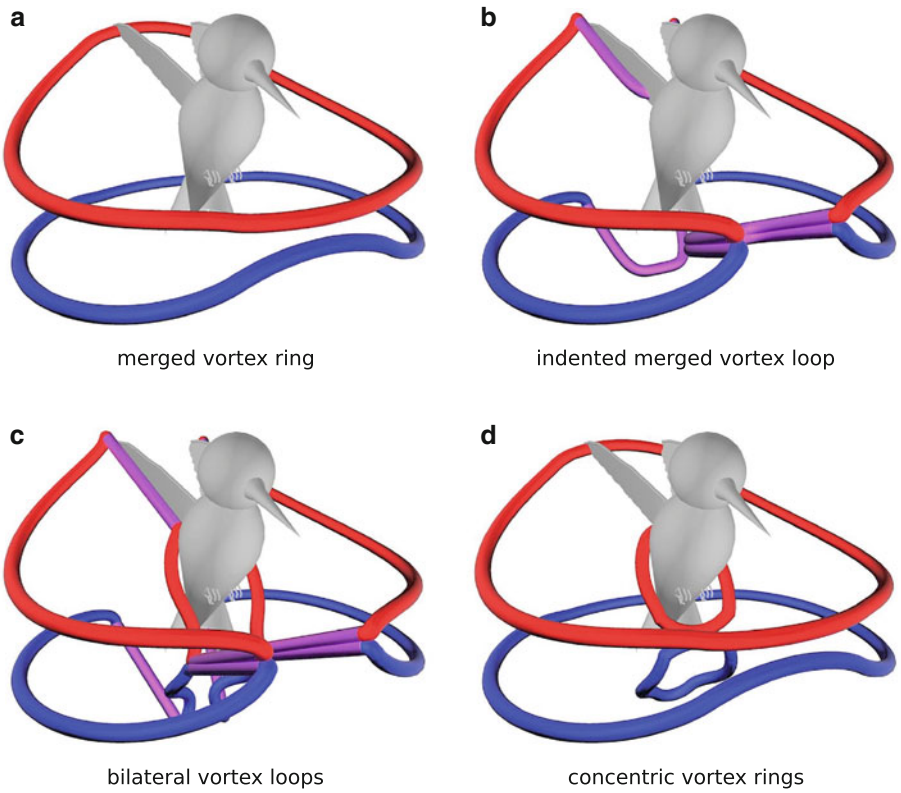

Fig. 5 Schematic representations of the simplified vortex topologies. For all four topologies, the downstrokes are indicated in *blue* and upstrokes are indicated in *red*. The merged vortex ring model (**a**) is similar to the structures shed from a helicopter. The indented, merged vortex loop model (**b**) can account for wingtip and reversal vortices (*purple*), but has a junction at the proximal region of the latter in place of root vortices. The bilateral vortex loop model (**c**) accounts for wingtip, wing root, and reversal vortices. The concentric vortices model (**d**) may occur at wing stroke amplitudes approaching 180°

1978; Feinsinger et al. 1979). An exciting prospect of the new topology of the hovering wake is that this may also contribute to new understanding of hummingbird physiological ecology.

4.2 Wingbeat kinematics

When hovering in normal air, hummingbirds used an average wing stroke amplitude of 153.6°, but the average stroke amplitude of the birds studied in the white plumes was only 129.8°. It has been demonstrated that hummingbirds will modulate stroke amplitude and wingbeat frequency under a variety of conditions (Ortega-Jimenez and Dudley 2012) and can match the lift requirements for different environmental and experimental conditions. Across taxa, high-elevation hummingbirds use higher stroke amplitudes during hovering than low-elevation taxa (Altshuler and Dudley 2003; Altshuler et al. 2010a). Measurements of the same taxa at different elevations reveal that hovering stroke amplitudes can increase by as much as 24° over a 1,000-m gain in elevation (Buermann et al. 2011). During experimental reduction of air density, hovering Ruby-throated hummingbirds *Archilochus colubris* increase stroke amplitude from $\sim$155° to a geometric limit near 180° (Chai and Dudley 1995). Hummingbirds challenged to hover when loaded with weights increase their stroke amplitudes up to the $\sim$180° limit from hovering values that are between 22° and 40° lower depending on the species (Chai et al. 1997; Chai and Millard 1997; Altshuler and Dudley 2003). Although it is reasonable to assume that hummingbirds will have bilateral vortex loops when using stroke amplitudes typical of hovering in normal air, this flow pattern could change as the wing stroke amplitude approaches 180°. The vortices shed from the two wings will approach each other as the stroke amplitude increases and may cancel each other out when the parallel reversal vortices collide. Under such circumstance, we hypothesized that the wake topology could consist of a root vortex ring, positioned within a wing tip vortex ring (Fig. 5d).

When hovering in the plume, the hummingbirds used lower stroke amplitudes but *higher* wingbeat frequencies on average. What could cause such an obvious change in wingbeat kinematics? We tested one hypothesis that the plume could be influencing the air density by comparing the recorded frequency of a Galton whistle (after Dudley 1995) in air and within the plume, as well as within larger clouds of dry ice, and within an airtight chamber. We did not detect any changes in air density greater than 1 %. It is also possible that a higher concentration of CO_2 could influence wingbeat kinematics by compromising oxygen metabolism. However, the higher wingbeat frequencies within the plume must derive from an increase in the contractile frequencies of the oxygen-demanding power muscles, which does not support this hypothesis. Instead, reductions in oxygen availability cause decrease in wingbeat frequency without a consistent effect on wing stroke amplitude during hovering flight in hummingbirds (Altshuler and Dudley 2003). Thus, the cause of the lower stroke amplitudes is presently unknown, but we propose that the higher wingbeat frequency may be a behavioral adjustment to allow for a rapid escape from an environment with reduced visibility and that maintaining vertical position with an elevated wingbeat frequency will necessarily require lower stroke amplitude.

Acknowledgments We thank Benny Goller for assistance with data collection and thoughtful discussions about the research. David Lentink, Dimitri Skandalis and three anonymous reviewers provided helpful comments on the manuscript. Lev Darkhovsky and Jonathan Scott assisted with animal care. This research was supported by grants from the United States National Science Foundation (IOS 0923849) and the Natural Sciences and Engineering Research Council of Canada (402677).

References

Altshuler DL, Dudley R (2003) Kinematics of hovering hummingbird flight along simulated and natural elevational gradients. J Exp Biol 206:3139–3147

Altshuler DL, Princevac M, Pan H, Lozano J (2009) Wake patterns of the wings and tail of hovering hummingbirds. Exp Fluids 46:835–846

Altshuler DL, Dudley R, Heredia SM, McGuire JA (2010a) Allometry of hummingbird lifting performance. J Exp Biol 213:725–734

Altshuler DL, Welch KC, Cho BH, Welch DB, Lin AF, Dickson WB, Dickinson MH (2010b) Neuromuscular control of wingbeat kinematics in Anna's hummingbirds (*Calypte anna*). J Exp Biol 213:2507–2514

Anderson JD (1991) Fundamentals of aerodynamics, 2nd edn. McGraw Hill, New York

Bomphrey RJ, Lawson NJ, Harding NJ, Taylor GK, Thomas ALR (2005) The aerodynamics of *Manduca sexta*: digital particle image velocimetry analysis of the leading-edge vortex. J Exp Biol 208:1079–1094

Bomphrey RJ, Lawson NJ, Taylor GK, Thomas ALR (2006) Application of digital particle image velocimetry to insect aerodynamics: measurement of the leading-edge vortex and near wake of a Hawkmoth. Exp Fluids 40:546–554

Bomphrey RJ, Taylor GK, Thomas ALR (2009) Smoke visualization of free-flying bumblebees indicates independent leading-edge vortices on each wing pair. Exp Fluids 46:811–821

Buermann W, Chaves JA, Dudley R, McGuire JA, Smith TB, Altshuler DL (2011) Projected changes in elevational distribution and flight performance of montane Neotropical hummingbirds in response to climate change. Glob Change Biol 17:1671–1680

Chai P, Dudley R (1995) Limits to vertebrate locomotor energetics suggested by hummingbirds hovering in heliox. Nature 377:722–725

Chai P, Millard D (1997) Flight and size constraints: hovering performance of large hummingbirds under maximal loading. J Exp Biol 200:2757–2763

Chai P, Chen JS, Dudley R (1997) Transient hovering performance of hummingbirds under conditions of maximal loading. J Exp Biol 200:921–929

Dickinson MH, Lehmann F-O, Sane SP (1999) Wing rotation and the aerodynamic basis of insect flight. Science 284:1954–1960

Dudley R (1995) Extraordinary flight performance of orchid bees (Apidae: Euglossini) hovering in heliox (80% He/20% O2). J Exp Biol 198:1065–1070

Ellington CP (1984) The aerodynamics of hovering insect flight. V. A vortex theory. Phil Trans R Soc Lond B 305:115–144

Epting RJ, Casey TM (1973) Power output and wing disc loading in hovering hummingbirds. Am Nat 107:761–765

Feinsinger P, Chaplin SB (1975) On the relationship between wing disc loading and foraging strategy in hummingbirds. Am Nat 109:217–224

Feinsinger P, Colwell RK (1978) Community organization among neotropical nectar-feeding birds. Am Zool 18:779–795

Feinsinger P, Colwell RK, Terborgh J, Chaplin SB (1979) Elevation and the morphology, flight energetics, and foraging ecology of tropical hummingbirds. Am Nat 113:481–497

Green SI (ed) (1995) Fluid vortices. Kluwer Academic Publishers, Dordrecht

Hedenström A, Johansson LC, Wolf M, von Busse R, Winter Y, Spedding GR (2007) Bat flight generates complex aerodynamic tracks. Science 316:894–897

Hedenström A, Muijres FT, von Busse R, Johansson LC, Winter Y, Spedding GR (2009) High-speed stereo DPIV measurement of wakes of two bat species flying freely in a wind tunnel. Exp Fluids 46:923–932

Hedrick TL (2008) Software techniques for two- and three-dimensional kinematic measurements of biological and biomimetic systems. Bioinspir Biomim 3:034001

Henningsson P, Muijres FT, Hedenström A (2011) Time-resolved vortex wake of a common swift flying over a range of flight speeds. J R Soc Interface 8:807–816

Hubel TY, Riskin DK, Swartz SM, Breuer KS (2010) Wake structure and wing kinematics: the flight of the lesser dog-faced fruit bat, *Cynopterus brachyotis*. J Exp Biol 213:3427–3440

Hubel TY, Hristov NI, Swartz SM, Breuer KS (2012) Changes in kinematics and aerodynamics over a range of speeds in *Tadarida brasiliensis*, the Brazilian free-tailed bat. J R Soc Interface 9:1120–1130

Johansson LC, Hedenström A (2009) The vortex wake of blackcaps (*Sylvia atricapilla* L.) measured using high-speed digital particle image velocimetry (DPIV). J Exp Biol 212:3365–3376

Kokshaysky NV (1979) Tracing the wake of a flying bird. Nature 279:146–148

Muijres FT, Johansson LC, Barfield R, Wolf M, Spedding GR, Hedenström A (2008) Leading-edge vortex improves lift in slow-flying bats. Science 319:1250–1253

Muijres FT, Johansson LC, Winter Y, Hedenström A (2011) Comparative aerodynamic performance of flapping flight in two bat species using time-resolved wake visualization. J R Soc Interface 8:1418–1428

Muijres FT, Bowlin MS, Johansson LC, Hedenström A (2012) Vortex wake, downwash distribution, aerodynamic performance and wingbeat kinematics in slow-flying pied flycatchers. J R Soc Interface 9:292–303

Norberg U, Kunz T, Steffensen J, Winter Y, von Helversen O (1993) The cost of hovering and forward flight in a nectar-feeding bat, *Glossophaga soricina*, estimated from aerodynamic theory. J Exp Biol 182:207–227

Ortega-Jimenez VM, Dudley R (2012) Flying in the rain: hovering performance of Anna's hummingbirds under varied precipitation. Proc R Soc B 279:3996–4002

Pennycuick CJ (1988) On the reconstruction of Pterosaurs and their manner of flight, with notes on vortex wakes. Biol Rev 63:299–331

Rayner JMV (1979) A vortex theory of animal flight. Part 1. The vortex wake of a hovering animal. J Fluid Mech 91:697–730

Rayner JMV, Gordon R (1998) Vizualization and modelling of the wakes of flying birds. Biona Rep 13:165–173

Spedding GR (1987) The wake of a kestrel (*Falco tinnunculus*) in flapping flight. J Exp Biol 127:59–78

Spedding GR, Rayner JMV, Pennycuick CJ (1984) Momentum and energy in the wake of a pigeon (*Columba livia*) in slow flight. J Exp Biol 111:81–102

Spedding GR, Rosén M, Hedenström A (2003) A family of vortex wakes generated by a thrush nightingale in free flight in a wind tunnel over its entire natural range of flight speeds. J Exp Biol 206:2313–2344

Stolpe M, Zimmer K (1939) Der schwirrflug des kolibri im zeitlupenfilm. J Ornithol 87:136–155

Wang XX, Wu ZN (2010) Stroke-averaged lift forces due to vortex rings and their mutual interactions for a flapping flight model. J Fluid Mech 654:453–472

Warrick DR, Tobalske BW, Powers DR (2005) Aerodynamics of the hovering hummingbird. Nature 435:1094–1097

Warrick DR, Tobalske BW, Powers DR (2009) Lift production in the hovering hummingbird. Proc R Soc B 276:3747–3752